Supplementary information for multi-prior physics-enhanced neural network for high-fidelity arbitrary-path optical particle manipulation

Yuxiang Yun1,2†, Wenyu Gao2,3†, Yuan Zhou2†, Xiaohao Xu2,3, Xuan Tian2,3, Siying Wang2,3, Shuquan Fei2,3, Runze Li2, Tong Peng2, Yanan Cai1*, Chen Bai2,3*, Baoli Yao2,3*

[1] Northwest A&F University, College of Science, Yangling 712100, China

[2] State Key Laboratory of Ultrafast Optical Science and Technology, Xi’ an Institute of Optics and Precision Mechanics, Chinese Academy of Sciences, NO.17 Xinxi Road, Xi’an 710119, China

[3] University of Chinese Academy of Sciences, Beijing 100049, China

†These authors contributed equally to this work

*caiyanan@nwafu.edu.cn

*baichen@opt.ac.cn

*yaobl@opt.ac.cn

Clarify the roles of priors with an ablation study

The proposed multi-prior framework integrates four complementary physical and structural constraints, each addressing a distinct aspect critical for generating high-quality optical conveyor belts. The Physical Consistency Prior enforces strict adherence to Richards-Wolf vector diffraction theory, providing an accurate model for computing the focused electric field and resultant optical forces. The Intensity Smoothness Prior suppresses local intensity spikes and speckle noise along the target path, enforcing uniform illumination essential for stabilizing gradient forces. The Phase Periodicity Prior resolves 2π phase ambiguity by mapping phase values onto a unit circle and employing a cyclic loss function, *e.g.*, cosine similarity, thereby ensuring continuous phase gradients without wrapping discontinuities—a prerequisite for

consistent phase-gradient forces. The Deep Image Prior leverages the intrinsic inductive bias of the convolutional architecture itself, rather than an external constraint, to favor smooth and physically plausible patterns. This architectural bias guides optimization toward realistic solutions even without explicit regularization and, in concert with the Phase Periodicity Prior, ensures stable, smooth phase-gradient forces along arbitrary trajectories. Consequently, these priors are complementary and non-redundant.

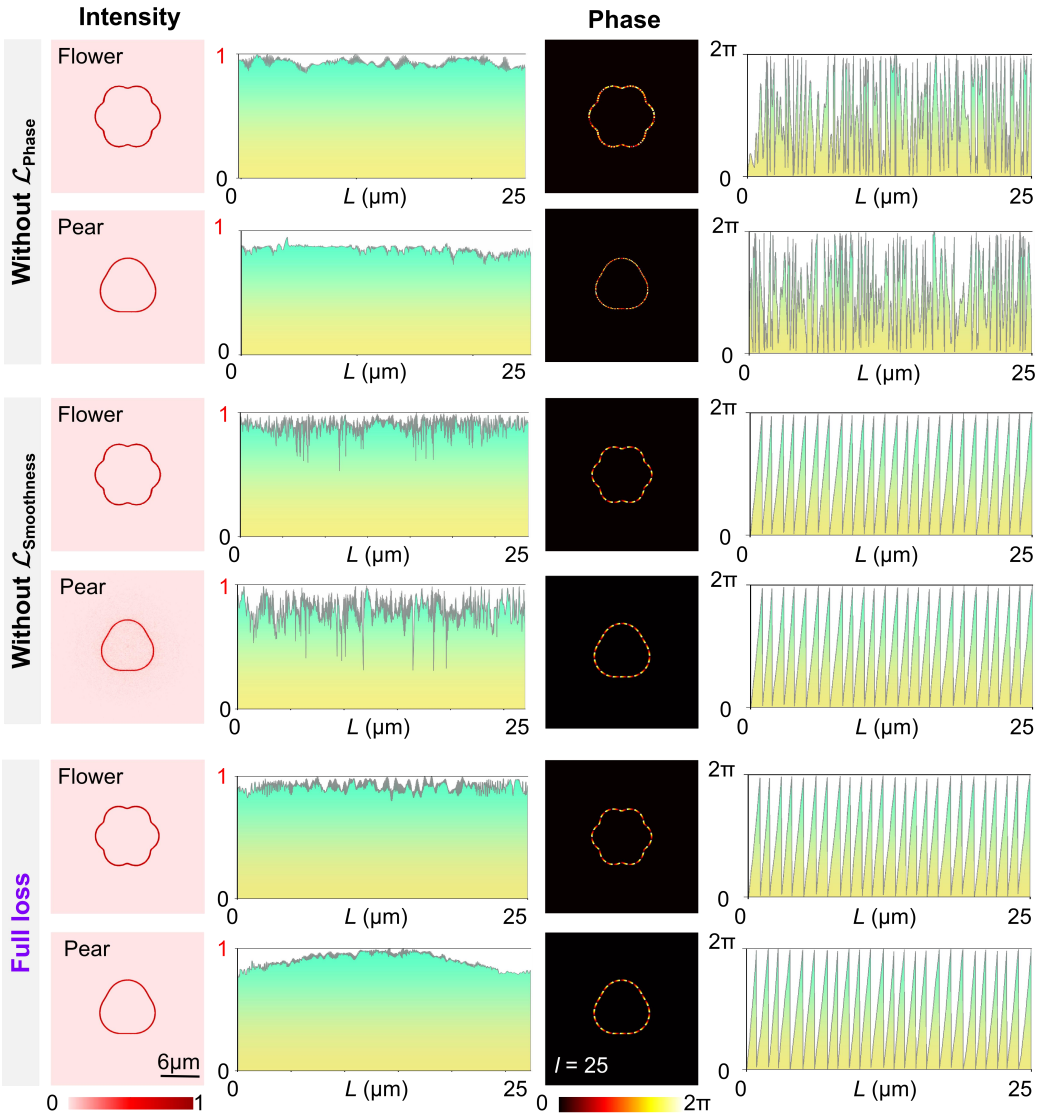

Figure S1. Ablation study on the effect of multi-prior loss components in MPPN-RW. Comparison of optical conveyor belt reconstruction results obtained without the phase periodicity loss (Λ_{Phase}), without the intensity smoothness loss ($\Lambda_{Smoothness}$), and using the full multi-prior loss. Two representative closed-loop transport trajectories, including a flower-shaped and a pear-shaped path, are evaluated.

To demonstrate the necessity of each component, we conducted ablation experiments on the

intensity smoothing and phase periodicity priors (note that the deep image prior is inherent to the network architecture, while the physical consistency prior is integral to the framework, precluding their ablation in the same manner). Analysis of Fig. S1 reveals that without the phase consistency loss Λ_{Phase}, the reconstructed phase exhibits pronounced random fluctuations along the trajectory, despite largely preserved intensity uniformity, indicating deficient phase controllability. Conversely, omission of the smoothness regularization loss $\Lambda_{\text{smoothness}}$ yields substantial intensity oscillations, particularly in high-curvature regions. The complete MPPN-RW framework, by contrast, produces markedly uniform intensity distribution and smooth, monotonically evolving phase profiles across both test trajectories. These findings collectively demonstrate the necessity and effectiveness of jointly incorporating phase consistency and smoothness priors for generating stable and physically meaningful optical transport fields.

Extendibility to other particle systems

The MPPN-RW method is an improved strategy for computational hologram optimization that customizes vortex optical fields along arbitrary trajectories while ensuring high intensity and uniform phase-gradient distributions, yielding more uniform orbital angular momentum flow. Fundamentally, the generated fields are generalized vortex beams. Gold particles were selected primarily to validate the hologram optimization method's effectiveness. Extensive studies have demonstrated manipulation of dielectric particles—including polystyrene, silica, and yeast cells—using generalized vortex beams, suggesting that our approach is readily extendable to other particle systems.[1, 2, 3]

To directly examine material dependence, we conducted numerical simulations for gold (Au), polystyrene (PS), and silica (SiO_2) particles under identical optical conveyor belt fields. The results (Shown as Fig. S2) demonstrate that all three particle types experience consistent and stable transverse optical forces along the designed trajectory, confirming that transport performance is not significantly affected by material differences. In fact, gold particles were deliberately selected for initial experimental validation due to their strong optical response and high scattering efficiency, which facilitate clear visualization of transport dynamics while providing a sensitive, robust test of the method's core functionality.

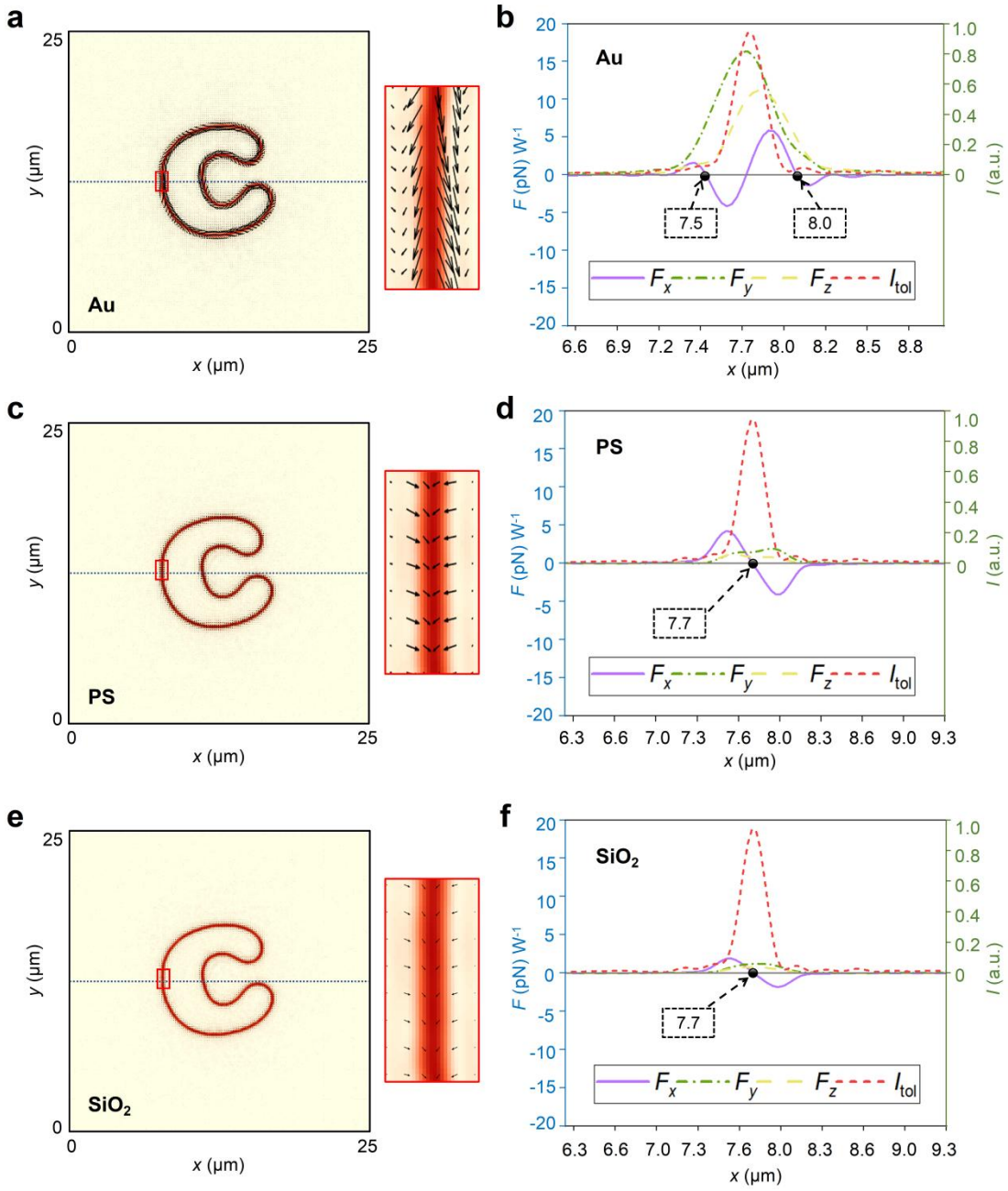

Figure S2. Transverse optical force distributions for particles with different refractive indices along a C-shaped optical conveyor belt generated by MPPN-RW. (a, c, e) Transverse optical force distributions for gold (Au), polystyrene (PS), and silica (SiO_2) particles (radius $R = 0.5$ μm), respectively. Arrows indicate the direction and magnitude of optical forces; insets show magnified views of the force distributions within the red-boxed regions. (b, d, f) Profiles of the total intensity $\boldsymbol{I}_{tol}$ (red curves), horizontal optical force $\boldsymbol{F}_x$ (purple curves), vertical optical force $\boldsymbol{F}_y$ (green curves), and axial scattering force $\boldsymbol{F}_z$ (yellow curves) along the blue dashed lines marked inside the red boxes in (a, c, e). Dark circles denote trapping positions.

In addition, we conducted supplementary directional transport experiments using pear-shaped and flower-shaped optical conveyor belts generated by the MPPN-RW framework for

~3.3 μm Polystyrene (PS) microspheres, SiO_2 microspheres, and yeast cells (~3-5 μm in diameter), as shown in Fig. S3 and Visualization 2. The experimental results demonstrate that, without requiring any fundamental modifications to the optical field design, the proposed method can be effectively extended to dielectric particles and biological cells, thereby confirming its strong generality and applicability.

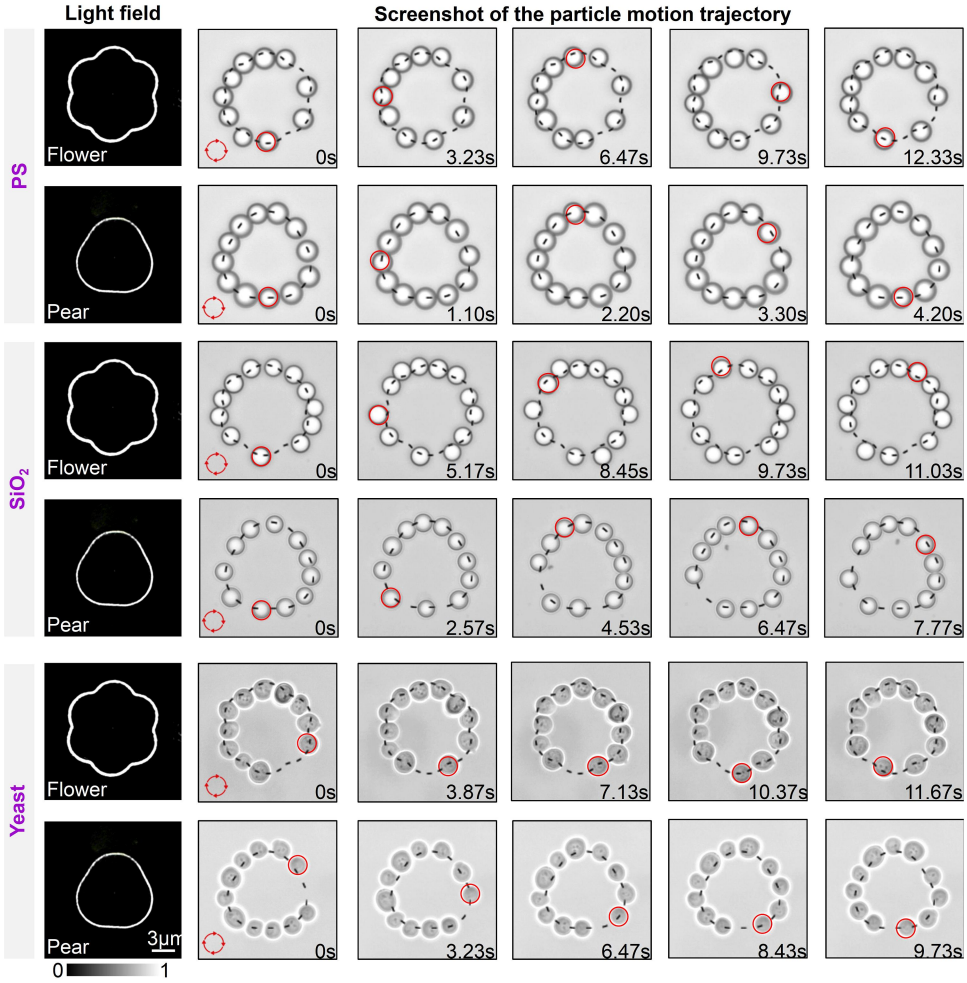

Figure S3. Experimental demonstration of particle transport along flower-shaped and pear-shaped optical trajectories generated by the MPPN-RW method (l = 25) (Visualization 2). Transport of PS microspheres, SiO_2 microspheres, and yeast cells is shown. The first column presents the light field intensity distributions, while the middle columns show time-lapse snapshots trapping the transport dynamics of the various particles.

Details of reconstruction runtime and convergence curves

On average, reconstructing a single trajectory using an Intel Xeon W-2223 CPU (16 GB RAM) and an NVIDIA T1000 GPU takes approximately 10 minutes (based on 4000 iterations to ensure absolute convergence). Here, we provide the convergence curves of the MPPN-RW optimization

process for both the pear-shaped and flower-shaped trajectories, shown as Fig. S4, with the total loss, intensity loss, and phase loss functions, specifically.

Our method fundamentally differs from training-based deep learning methods and conventional iterative approaches. Training-based methods require large datasets for offline training, which is impractical for high-NA tightly focused optical fields due to limited generalization. Furthermore, standard iterative optimization methods are typically limited to a narrow set of constraints and cannot simultaneously enforce multiple physical priors—such as intensity uniformity, strict phase-gradient continuity, and adherence to vector diffraction physics—that are critical for stable particle transport along arbitrary paths. In contrast, the proposed MPPN-RW framework is entirely training-free. It directly performs trajectory-specific optimization by integrating a fully differentiable vector diffraction model with a multi-prior loss function. This physics-driven approach efficiently converges to solutions suitable for optical manipulation, overcoming the data limitations and constraint incompleteness of other methods to provide a practical, robust solution for high-NA, phase-gradient-driven particle transport.

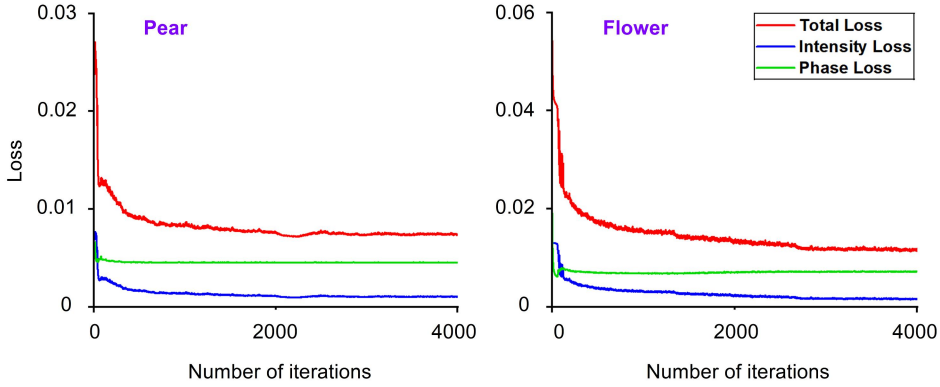

Figure S4. Convergence behavior of the MPPN-RW optimization process. Evolution of total loss (red), intensity loss (blue), and phase loss (green) with respect to iteration number. The left and right panels correspond to pear- and flower-shaped optical conveyor belts, respectively. Despite their distinct geometries, all loss components converge stably and consistently, reflecting effective joint optimization of intensity and phase constraints. Occasional loss spikes result from intentional perturbations introduced to escape local minima, following which the optimization rapidly reconverges to lower loss values. The smooth decay and ultimate saturation of all loss terms collectively demonstrate the robustness and stability of the proposed physics-enhanced multi-prior optimization framework.

Multi-Prior Weighting Coefficient Selection (λ values)

The weighting coefficients of the multi-prior loss function (λ_{Phy}, λ_{Smo}, λ_{Per}) play a critical role in ensuring the robustness, reproducibility, and potential extensibility of the proposed MPPN-RW framework across different trajectories and experimental conditions. In this work, these coefficients were determined through a limited number of preliminary exploratory trials, aiming

to balance the contributions of the deep-physics prior, smoothness prior, and phase prior. Once selected, the same set of coefficients was fixed and applied consistently across all reconstruction tasks, without trajectory-specific tuning. Under this fixed λ setting, the model exhibited stable convergence and reliable reconstruction performance for both closed and non-closed trajectories, indicating that the chosen coefficients are not overly sensitive to the specific geometry of the trajectory.

Experimental Robustness and Performance Analysis

To mitigate phase errors from the spatial light modulator (SLM), we implemented a dedicated phase calibration procedure. Since the SLM employed in our experiment is essentially a liquid-crystal-based electro-optic modulation device, its input electrical signal (gray level) and the resulting optical intensity modulation generally exhibit a nonlinear relationship. Therefore, before the experiments, a calibration procedure is required to compensate for this intrinsic nonlinearity. Specifically, the optical response of the SLM was first measured over the full range of gray levels to obtain its inherent response curve. Based on this measured curve, an inverse correction look-up table (LUT) was constructed. During operation, the target gray values generated by the control system were pre-distorted using this LUT, such that the effective output of the SLM closely matches the theoretical design values. [4, 5] Furthermore, to mitigate aberrations introduced by the SLM, a first-order Laguerre–Gaussian beam was employed as a reference wavefront for phase evaluation. By optimizing the coefficients of Zernike polynomials, we successfully corrected system aberrations, [6] as shown in Fig. S5. Besides, a blazed grating phase was embedded into the hologram, which effectively filtered out stray and zero-order light originating from hologram inaccuracies and the SLM's intrinsic structure. Additionally, a highly stable continuous-wave fiber laser (VFLS-1064-B-SF-HP) was used for its excellent power stability, thereby minimizing experimental interference from laser fluctuations.

Concerning the stability during transport, the transfer of spin angular momentum from the circularly polarized light induces a spin in the metallic particles. This can lead to fluctuations in their rotational speed, a phenomenon consistent with the known spin-orbit coupling mechanism.[7, 8] As for the observed trajectory deviation, we found that the actual path of the gold particles does not align with the intensity peak. Instead, they travel along the inner or outer edge of the prescribed trajectory, a behavior also replicated in our numerical simulations. This is attributed to the "gray optical trapping" effect caused by multipole gradient forces, which confines particles

to regions of non-extreme light intensity.[9] It is noteworthy that this effect is significantly weaker for dielectric particles (e.g., SiO_2 and PS microspheres). Consequently, as demonstrated in Fig. S2, these particles adhere closely to the trajectory defined by the prescribed optical intensity profile.

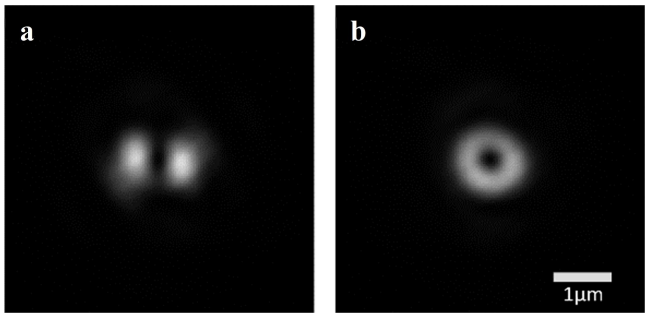

Figure S5. Experimentally measured intensity distributions of a Laguerre-Gaussian (LG) vortex vortex (l = +1). **a,** Before correction. **b,** After correction.

Relationship Between Field Uniformity Metrics and Transport Stability

To explicitly link the quantitative metrics to the observed transport behavior, we added a statement, clarifying that a lower intensity coefficient of variation (CV) suppresses local fluctuations in the gradient forces, while improved phase-gradient uniformity ensures smooth and continuous optical force directions. Together, these effects mitigate particle stagnation and reduce trajectory deviations, particularly in high-curvature regions, thereby providing a clearer physical interpretation of how the field properties contribute to enhanced transport stability.

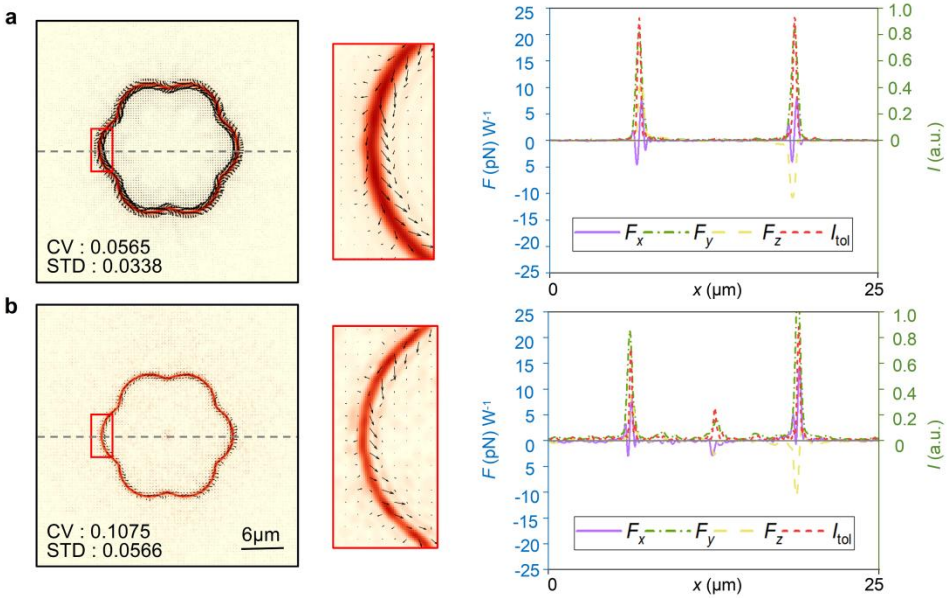

Figure S6. Optical force distributions and intensity profiles for gold particles under tightly focused structured light fields along representative trajectories. **a,** High-fidelity trajectory with low intensity variation (CV = 0.0565) and phase standard deviation (STD = 0.0338). The left panel shows the intensity distribution overlaid with optical force vectors (black arrows), with the inset highlighting the local force directions along the curved segment. The right panel depicts the force components (F_x, F_y, F_z) and the normalized total intensity ($\boldsymbol{I}_{\mathrm{tol}}$) along the horizontal cross-section indicated by the dashed line. **b,** Lower-fidelity trajectory with higher intensity variation (CV = 0.1075) and phase standard deviation (STD = 0.0566).

To clarify this issue, we conducted a comparative force analysis on gold particles ($R = 0.5$ μm) using two distinct flower-shaped optical conveyor belts: one with a higher intensity coefficient of variation (CV = 0.1075) and phase standard deviation (STD = 0.0566), and the other with lower values (CV = 0.0565, STD = 0.0338). As shown in Fig. S6, the lower CV and STD correspond to a more uniform intensity profile and a smoother phase gradient, which in turn stabilize the optical forces and minimize particle drift along the trajectory. These findings underscore that maintaining low CV and STD is essential for achieving smooth optical forces and reliable particle transport in high-numerical-aperture optical fields.

References

1. Wei, W. et al. Cycloid-structured optical tweezers. Opt. Lett. **48**, 972–975 (2023).
2. Yun, X. et al. High-efficiency generation of long-distance, tunable, high-order nondiffracting beams. Photon. Res. **12**, 2390–2400 (2024).
3. Zhu, L. et al. Optical vortex lattice: an exploitation of orbital angular momentum. Nanophotonics **10**, 2487–2496 (2021).
4. Li, R. et al. Progress in phase calibration for liquid crystal spatial light modulators. Applied Sciences **9**, 2012 (2019).
5. Zhao Y. et al. High-precision calibration of phase-only spatial light modulators. IEEE Photonics J. **14**, 1-8 (2021).
6. Liang, Y. et al. Aberration correction in holographic optical tweezers using a high-order optical vortex. Appl. Opt. **57**, 3618-3623 (2018)
7. Friese, M. E. J. et al. Optical angular-momentum transfer to trapped absorbing particles. Phys. Rev. A **54**, 1593 (1996).
8. Lehmuskero, A. et al. Ultrafast spinning of gold nanoparticles in water using circularly polarized light. Nano Lett. **13**, 3129–3134 (2013).

9. Zhang, Y. et al. Full-gray optical trapping by high-order multipole-resonant gradient forces in structured light. Phys. Rev. A **110**, 063517 (2024).